# Online Rolling Evolutionary Decoder-Dispatch Framework for the Secondary Frequency Regulation of Time-varying Electrical-Grid-Electric-Vehicle System

Chaoyu Dong, Ronghe Chu, Thomas Morstyn*, *Member, IEEE*, Malcolm D. McCulloch, *Senior Member, IEEE*, Hongjie Jia*, *Senior Member, IEEE*

***Abstract*—The widespread integration of electric vehicles (EVs) into the electrical grid creates a new opportunity for frequency regulation. In this paper, to deal with the penetration of intermittent renewable energy and the time variance of system model, an online evolutionary mechanism is developed for the electrical-grid-electric-vehicle system. With a real-time decoder consisting of the long-short-term memory (LSTM) array, the dispatch center is upgraded from a passive executor to an intelligent analyst, which extracts the rolling features from multiple time scales. Based on the high-dimension decoding information from the LSTM array, a deep neural network (DNN) array is then embedded to provide strategic dispatch commands learning from the evolving memory. The whole decoder-dispatch framework is then upgraded with a unified online adaption technique to achieve gradient optimization and weight evolution. The proposed evolutionary structure is validated on a frequency management system to demonstrate its superior performance.**

***Index Terms*— online dispatch algorithm, long-short-term memory-deep neural network (LSTM-DNN) array, electric vehicles, electrical grid.**

## I. Introduction

TIME-VARYING renewable energies are rapidly penetrating the conventional electrical system, which reduces the share of provided by thermal generators. It was reported that renewable energies including wind and solar are contributing more than 20% of supply in Germany and Denmark [1]. Targeting at least 80% renewable electricity by 2050, the large-scale integration of renewable energy sources has been supported by the German Renewable Energy Sources Act in Germany [2]. By 2020, according to Danish Energy Agency, the binding renewable objectives for Denmark are a total renewables share of 30%, a renewable share of 10% in transport, and a 20% carbon reduction [3]. Although the energy transition would slow down global warming and fossil fuel consumption, the variability and fluctuation introduced by the solar and wind have become significant issues for the electrical grid due to the changeable weather, various locations, different devices, etc. From the measurement data of Electric Power Research Institute (EPR) in June 2012 [4], a 190kW PV system experienced frequent variation during the 7 am-12 pm, with the ramp rate reaching 23kW per second in Fig. 1. Considering the increasing penetration of renewable energy, the risk and uncertainties caused by stochastic renewable generation can no longer be neglected.

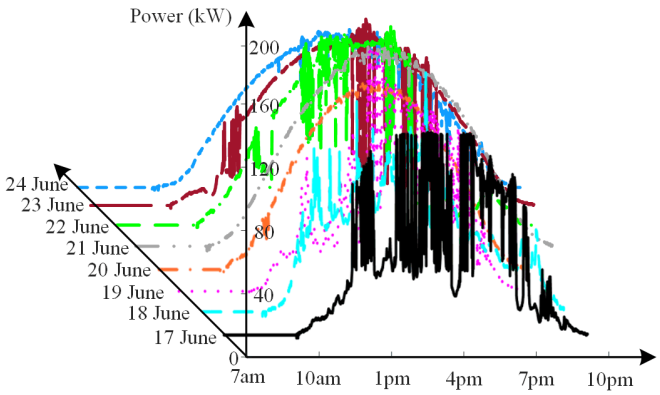


Fig. 1. The PV power variations of 8 days in June, 2012.

Besides these energy trends, the acceleration of transport electrification is also reconfiguring the electrical grid. It was reported that the incorporation of electric vehicles (EV) into electrical power systems would provide a new means of increasing system reliability [5]. Since 2006, the Chinese government has been setting the development of electric vehicles as priority themes in the national long-term development plan (2006–2020) [6]. The proper arrangement of EV loads may benefit the utility by shaving peaks, filling valleys, and absorbing renewable energy generation. However, various vehicle types and traveling purposes lead to variations

This work is supported in part by the National Natural Science Foundation of China under Grant 51625702 and in part by the Joint Fund Project of National Natural Science Foundation-State Grid Corporation under Grant U1766210. (Corresponding authors: Thomas Morstyn and Hongjie Jia)

C. Dong is with Energy Research Institute@NTU, R. Chu, and H. Jia are with School of Electrical and Information Engineering at the Tianjin University and Key Laboratory of Smart Energy and Information Technology of Tianjin Municipality, Tianjin 300072, China. (email: dongchaoyuyd@gmail.com, chu_rh@tju.edu.cn, hjjia@tju.edu.cn).

T. Morstyn is with the School of Engineering at the University of Edinburgh, Edinburgh EH9 3JL, United Kingdom (email: Thomas.Morstyn @ed.ac.uk).

M. D. McCulloch is with the Department of Engineering Science at the University of Oxford, Oxford OX1 2JD, United Kingdom (email: malcolm.mcculloch@eng.ox.ac.uk).

in the behaviors of EVs. Because of different driving plans and temporary tasks, the whole EV network would be time-varying most of the time [7], which could barely be described with one uniform and simple model. Moreover, on account of the electro-chemical-dynamics from heterogeneous batteries, battery capacities and charging rates varied with their health statuses, aging effects, and manufacturing processes [8]. Coupling with the parameter uncertainties of whole electrical grid, the online time variance of the grid-vehicle system would be more challenging, especially considering the predication burden from the intermittency of renewable energies.

Frequency is an important index in the electricity industry, which is directly related to the normal operation of the electrical-grid-electric-vehicle system, especially considering the growing penetration of stochastic renewable energy. When the low frequency nadir or high rate of frequency change occurs, the operation of electrical grid would suffer from unscheduled load curtailments, frequency crashes, cascading tripping, which might finally induce a large-scale outage for the whole system [9]. On 9-August-2019, a blackout was triggered in Britain with a severe dip of frequency to 48.88Hz. In less than an hour, around 936,000 people in England and Wales were affected, and travel across the country was disrupted and suspended [10]. Because of the increasing energy density and the sale volumes, EVs have the potential to participate in the secondary frequency regulation of the electricity grid. According to the regulation target and timescale [11], EVs could be involved in the primary, secondary, and tertiary frequency responses. By designing the EV charging modes, the power demands from EVs were adjusted to support the primary frequency control within 10-60 seconds [12]. Different from the primary response requirement facing short-term frequency changes within seconds, the secondary frequency regulation was a relatively long-term control, which employed EV to restore the grid scheduled frequency within the recovery period of 1-10 minutes [13]. For the economic benefits of EV aggregators, the vehicle power was optimized in 10-60 minutes [14]. Given the model unpredictability from EVs and renewable sources, and the large sum of economic losses, there is an urgent need to evolve the current frequency management system.

For the conventional electrical grid consisting of thermal generating units, linear methods such as integral or proportional-integral controllers were widely utilized as the secondary frequency regulation approaches [15]. Even if there is a small modification of the turbine from non-reheated type to reheated type [16], the performance of the original dispatch center based on linear methods would suffer due to the model dependence of controllers. Nonlinear techniques such as sliding mode control [17] and fuzzy logic system approach [18] have been exploited to achieve the load frequency control for the power system. To enhance the frequency regulation performance with vehicle-to-grid implementation, an optimized fuzzy controller was used in [19] to control EVs in the deregulated power system. Responding to the area control error, EV charging was controlled by fuzzy rules and membership functions to compensate for the power imbalance in the secondary frequency control [20]. By the single-hidden-layer neural network, [21] developed an adaptive controller for the frequency response of EVs. However, the employment of a single-hidden-layer neural network burdens the effective extraction of complex temporal feature. Moreover, these controllers are all based on either the original model or offline experience, to design the regulation laws, which are not able to evolve with their fixed parameters set offline. For the time-varying and heterogeneous electrical-grid-electric-vehicle system, the model difficulty and computational burden would further limit the applications of those methods. Furthermore, without self-learning and online adaptation mechanisms, the original dispatch center inflexibly regulates each frequency variation case, which not only leads to low dispatch efficiency but also is incompetent facing unknown circumstances.

Facing those challenges of internal variations and external intermittences, the original dispatch strategy needs to be simultaneously strengthened with an online decoder for evolutionary learning of system status and an executor for complex decision making that incorporates continuous and rolling system variations. From a passive executor to an active thinker, the long short-term memory (LSTM) network provides a feasible scheme for the decoder. As one type of recurrent neural network, Hochreiter and Schmidhuber proposed LSTM to efficiently store information over extended time sequences [22]. Inside the network, long-term and instantaneous memories organically interact, which successfully avoids the vanishing of error signal backpropagation. In [23], LSTM units were employed to identify the real-time power imbalance for Singapore's power system. In terms of energy user uncertainties, the short-term load forecasting was also achieved via LSTM [24]. With natural advantages on feature extraction, the deployment of LSTM array might have the potential to play the decoder role, accumulating fluctuation knowledge from the online frequency regulation. However, the online performance of LSTM array remains to be investigated.

On account of the high-dimension feature extracted from the time sequences and the various demands from different EV aggregators, the deep neural network (DNN) and its combination with the graphics processing unit (GPU) emerge as a promising answer for decision making dealing with real-time condition changes. In [25], deep recurrent neural network learning was presented to generate a near-optimal scheduling policy for the microgrid economy. To optimize the demand-side energy management, a DNN was trained based on the historical data to model the response from local operators [26]. With two contesting DNNs, the generative adversarial network was utilized to fill up PMU data for security assessment [27]. Meanwhile, the power of parallel computation from graphic processing units (GPUs) has been applied to several power system applications. [28] reported that the power flow computation speed can be 2.86 times faster with the help of GPU. The employment of gradient methods with a GPU was also suitable for speeding up complex computation [29]. The high efficiency and output effectiveness show DNN and GPU merits as a promising dispatcher interfacing LSTM. However, to our best knowledge, there is no clear report about their

application and computation results in online frequency management.

Motivated by these gaps, this paper proposes a decoder-dispatch framework based on the interconnection of LSTM and DNN, which formulates the closed dispatch loop for the frequency regulation. Apart from the decoder-dispatch paradigm, a rolling evolutionary method is also developed to gradually upgrade the dispatch center with real-time optimal gradient and the squared gradient. Through the separate design of two neural networks and the unified adaption of real-time scenarios, the rolling decoder-dispatch framework can be easily integrated with various existing techniques and objectives to test their management performance. In addition, the removal of offline training and the implementation of GPU further boosts the framework for online deployment.

This work is different from existing studies in the five aspects: 1) modular framework, 2) LSTM role, 3) DNN role, 4) online evolutionary mechanism, 5) comparison comprehensiveness and design workflow for the framework. From these five aspects, the contributions of this paper are summarized and explained as follows.

**1) Decoder-dispatch framework.** This paper decouples the complicated management task of the time-varying electrical-grid-electric-vehicle system considering the stochastic renewable energy, where a decoder-dispatch framework is established mimicking the human dispatcher loop. By this framework, various techniques can be simultaneously employed in the decoder module and dispatch module. However, in existing studies [19], [20], [21], their main concern is to design a better dispatch module offline. As an extension of their work, the decoder module for the extraction of time-sequence information and the online evolutionary mechanism are both investigated in this study.

**2) Temporal LSTM network learning.** Due to the temporal characteristics from the frequency deviation, the LSTM network is embedded in the decoding part, which evolves rolling memory with real-time circumstances. As an effective technique for the information extraction in the temporal order [22], the LSTM network was trained offline in [23] to identify the power fluctuation and in [24] to forecast the short-term residential load. Different from the fitting role in existing studies, the LSTM array is utilized as a temporal decoder for the frequency management in this work, which learns the high-dimension system feature during the continuous operation.

**3) DNN interface and dynamic dispatch.** Absorbing the high-dimension information, an intelligent DNN is interfaced with the LSTM output to generate the dispatch command playing as the decision-maker. With the stack of multiple layers, DNN has been trained in [25], [26], [27] to model the relationship between given inputs and outputs. However, the DNN array plays as the interface of the temporal network in this work, which generates the dispatch commands for the electrical-grid-electric-vehicle system.

**4) Rolling evolutionary mechanism.** Instead of a static regulator, a two-layer rolling mechanism is developed, which maximizes the LSTM analysis capacity in the first layer with rolling inputs and evolves the LSTM-DNN system gradient in the second layer. Previous researches in [21]-[26] usually implement sufficient training offline, but the proposed decoder-dispatch framework is implemented online. The rolling gradient backpropagation is performed in the whole network and activated only if the absolute and relative frequency deviations both exceed the thresholds.

**5) Complete validation tests and framework design workflow.** The complete validation tests are carried out from six aspects: renewable energy fluctuation, electrical grid variations, electric vehicle variations, comparisons with linear and nonlinear methods, compatibility with the existing approach, and robustness tests on different datasets. The design workflow for the framework parameters is also developed considering the features of frequency management and deep network.

Besides the demonstrated deep learning methods, the core idea of this work is to develop a unified online decoder-dispatch framework for the frequency management of the electrical-grid-electric-vehicle system. Following the proposed decoder-dispatch framework and demonstrated case studies, various techniques, including traditional controllers, deep learning methods, or even the integration of traditional and deep learning methods, can participate in the real-time dispatch task facing the increasing penetration of renewable energy and electrical-grid-electric- vehicle dynamics.

The remainder of this paper is as follows. In Section II, an outline of the electrical-grid-electric-vehicle system is presented as well as a review of the frequency regulation problem. In Section III, to address the problems of model uncertainty and disturbance randomness, a decoder-dispatch structure is then designed allocating the complicate task to LSTM and DNN, respectively. A two-layer rolling and online updating principle are developed in Section IV, which iterates two network interface and the whole dispatch center in parallel. Section V demonstrates the merits of proposed framework and online evolution mechanism on a typical frequency regulation system. Also, experimental results with GPU devices are presented. Finally, the conclusions are drawn in Section VI.

## II. System Structure and Frequency Problem

The penetration of intermittent renewable energy and the popularization of EVs are transforming the original electrical grid. In this section, the system configuration and the emerging frequency issue are reviewed.

### *A. Time-varying Electrical-Grid-Electric-Vehicle System*

The conventional frequency regulation system is shown in Fig. 2 with a grey color. Generators are aggregated as an equivalent generation unit consisting of the governor, reheat, and turbine [30]. Considering the lumped inertia $M(t)$ and damping $D(t)$ of power system, the grid frequency is derived as

$$\Delta\dot{f}(t) = -\frac{D(t)}{M(t)}\Delta f(t) + \frac{1}{M(t)}\Delta P_g(t) + \frac{1}{M(t)}\Delta P_r(t) \quad (1)$$

where $\Delta f(t)$, $\Delta P_g(t)$ are the time-varying frequency deviations

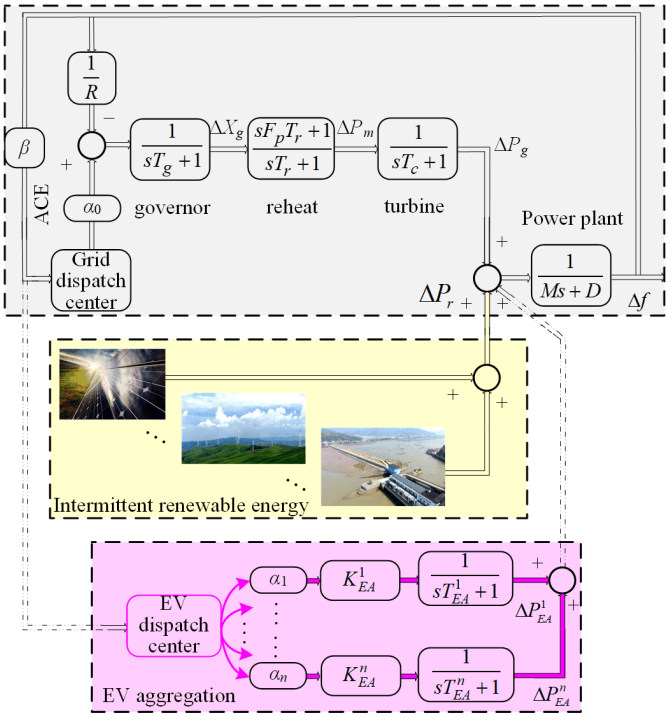


Fig. 2. Electrical-grid-electric-vehicle system.

and generator power output, respectively. Through $\Delta P_r(t)$, renewable energy intermittences from PVs, wind farms, and tidal power in yellow color are continuously injected into the grid disordering the whole system.

In Fig. 2, the time-varying incremental values of governor $\Delta X_g$, reheat $\Delta P_m$, and governor outputs $\Delta P_g$ in (2)-(4) also contribute to the system uncertainties

$$\Delta \dot{P}_g(t) = -\frac{1}{T_c(t)}\Delta P_g(t) + \frac{1}{T_c(t)}\Delta X_g(t) \tag{2}$$

$$\Delta \dot{P}_m(t) = \frac{-F_p(t)\Delta f(t)}{R(t)T_g(t)} - \frac{\Delta P_m(t)}{T_r(t)} + \frac{T_g(t)-F_p(t)T_r(t)}{T_r(t)T_g(t)}\Delta X_g(t) + \frac{F_p(t)\alpha_0}{T_g(t)}u(t) \tag{3}$$

$$\Delta \dot{X}_g(t) = -\frac{1}{R(t)T_g(t)}\Delta f(t) - \frac{1}{T_g(t)}\Delta X_g(t) + \frac{\alpha_0(t)}{T_g(t)}u(t) \tag{4}$$

where $T_c(t)$ is the time coefficient of turbine, $T_r(t)$ is the reheat time coefficient, $F_p(t)$ is the fraction of total turbine power, $T_g(t)$ is the time coefficient of governor actuator, $R(t)$ is the droop coefficient indicating the relationship between the frequency deviation and the gate position, $\alpha_0(t)$ denotes the participation ratio of aggregated thermal generator.

With the bias factor $\beta$, the area control error ACE($t$) signal of the power system is obtained as

$$\mathrm{ACE}(t) = \beta \Delta f(t) \tag{5}$$

The traditional dispatch command via proportional-integral (PI) controller is then formed based on the ACE signal [17]

$$u_{EG}(t) = -K_P ACE(t) - K_I \int ACE(t)dt \tag{6}$$

Besides the internal parameter variations of the electrical grid and the external renewable energy injection, the participation of EVs is aggregating to be the other variable energy group. Taking the simplified EV aggregators in [13] as examples, a large number of electric vehicles are simply described as the following first-order transfer function

$$G_{EV}^k(s) = \frac{K_{EV}^k(t)}{1 + sT_{EV}^k(t)} \tag{7}$$

where $K_{EV}^k(t)$ is the output gain of the $k^{th}$ EV aggregator, $T_{EV}^k(t)$ is the corresponding battery time efficiency. The power contribution from the $k^{th}$ aggregator ($k$=1,…, $n$) is

$$\Delta \dot{P}_{EV}^k(t) = -\frac{1}{T_{EV}^k(t)}\Delta P_{EV}^k(t) + \frac{\alpha_k K_{EV}^k(t)}{T_{EV}^k(t)}u_{EV}^k(t) \tag{8}$$

where $\alpha_k$ indicates the aggregator participation ratio.

With $\boldsymbol{x}_{EV}(t) = [\Delta P_{EV}^1(t), ..., \Delta P_{EV}^n(t)]^T$, the EV system dynamic is

$$\dot{\boldsymbol{x}}_{EV}(t) = \boldsymbol{A}_{EV}\boldsymbol{x}_{EV}(t) + \boldsymbol{B}_{EV}u_{EV}(t) \tag{9}$$

where $\boldsymbol{A}_{EV}(t) = diag\{-1/T_{EV}^1(t), \ldots, -1/T_{EV}^k(t), \ldots, -1/T_{EV}^n(t)\}$, $\boldsymbol{B}_{EV}(t) = diag\{-\frac{\alpha_1 K_{EV}^1(t)}{T_{EV}^1(t)}, \ldots, -\frac{\alpha_k K_{EV}^k(t)}{T_{EV}^k(t)}, \ldots, -\frac{\alpha_n K_{EV}^n(t)}{T_{EV}^n(t)}\}$.

With (1)-(9), the state-space model of the frequency regulation system is established

$$\dot{\boldsymbol{x}}(t) = \boldsymbol{A}(t)\boldsymbol{x}(t) + \boldsymbol{B}(t)\boldsymbol{u}(t) + \boldsymbol{F}(t)\Delta P_r(t) \tag{10}$$

where $\boldsymbol{x}_{EG}(t) = [\Delta f(t), \Delta P_g(t), \Delta X_g(t), \int \Delta ACE(t)dt]^T$, $\boldsymbol{x}(t) = [\boldsymbol{x}_{EG}, \boldsymbol{x}_{EV}]^T$, $\boldsymbol{u}(t) = [u_{EG}, \boldsymbol{u}_{EV}]^T$. The expressions for $\boldsymbol{A}(t)$, $\boldsymbol{B}(t)$, and $\boldsymbol{F}(t)$ are attached in Appendix A.

Despite several assumptions made to simplify the whole system, the electrical-grid-electric-vehicle system (10) still exist enormous parameter and model uncertainties seen from the $\boldsymbol{A}(t)$, $\boldsymbol{B}(t)$, and $\boldsymbol{F}(t)$. Not only lumped coefficients $D(t)$, $M(t)$, $T_c(t)$, $T_r(t)$, $T_g(t)$, $T_{EV}^1(t)$ ,…, $T_{EV}^n(t)$ , $T_g(t)$, $F_p(t)$ are hard to determine, the variability from $\Delta P_r(t)$ and EV aggregation time would both modify the system dimension and structure.

### *B. Frequency Problem*

As shown in (10), the system frequency suffers from the disturbances from three aspects:

1) Grid dynamics: During the real-time operation, it is difficult to reflect the huge grid with only (1)-(4). The limited equations can barely reflect complicated system dynamics and parameter values are continuously changing.

2) Random EV charging and discharging: With time-varying

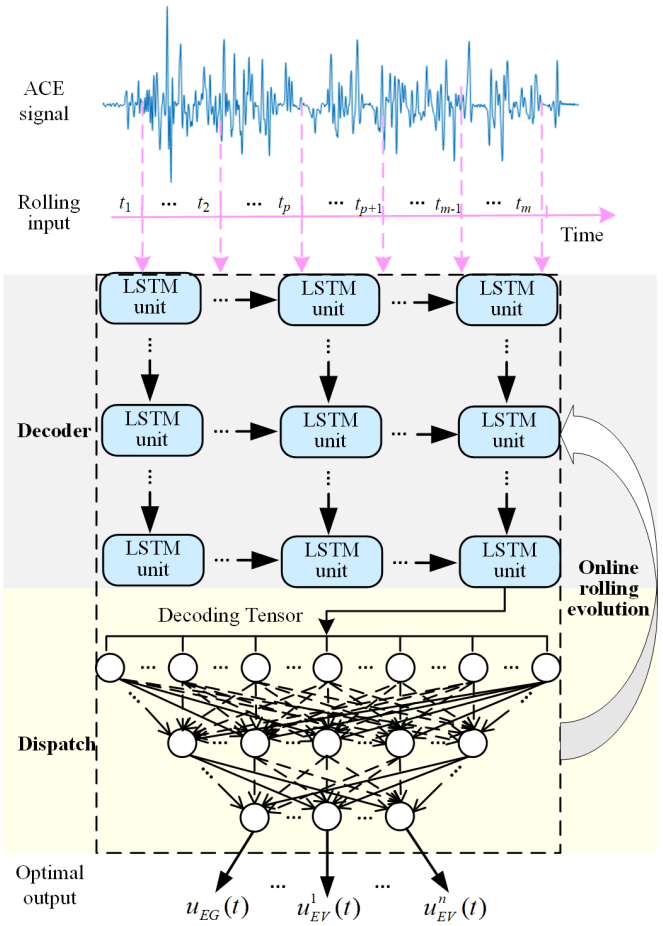


Fig. 3. Rolling evolutionary decoder-dispatch framework.

EV number and battery statuses, the representation accuracy of EV aggregation with a first-order transfer function (7) remains to be improved.

3) Renewable intermittence. Considering the stochastic resources such as solar, wind, tide in Fig. 2, the frequency variation would become more common with the higher level of renewable energy penetration.

To avoid the blackout risk caused by the frequency deterioration, the following traits are needed for the regulation:

1) Active analysis: The lack of accurate model hinders the optimization in advance. Moreover, the traditional approach passively manages the system according to the current ACE signal or frequency deviation, which is unable to make decisions based on the rolling signal variation.

2) Continuous adjustment: The instantaneous power fluctuation could reach more than 10% from Fig. 1, which is also different every day. The manual and duplicated dispatch scheme are both slow and inaccurate during responses.

3) Online evolution: Making use of past and real-time data is core in the decision-making process. Hence, it is necessary for the regulator to self-evaluate and renew its knowledge.

## III. Rolling Evolutionary Decoder-Dispatch Framework

In response to the complex tasks for frequency regulation, this section designs a rolling-evolutionary framework, shown in Fig. 3 for the electrical-grid-electric-vehicle system. This framework decouples the heterogeneous online management into three subsystems of decoder, dispatch, and evolution. The independent application of LSTM or DNN has been well-developed, which is trained offline for the classification or regression. On the basis of their advantages, i.e., LSTM for the temporal signal analysis and DNN for the big data processing, this paper extends their application in the secondary frequency dispatch and integrates these two types of neural networks for the implementation of proposed framework.

### A. Rolling Decoder Based on Deep LSTM Array

Considering the continuous frequency fluctuation, the deep long short-term memory (LSTM) [16] array is deployed in Fig. 3 as a decoder example extracting time-series information. The structure of the LSTM cell comprising the forget gate, update gate, output gate is shown in Fig. 4. With the weights $\boldsymbol{W}_{(f,\,u,\,o)}$ and bias $\boldsymbol{b}_{(f,\,u,\,o)}$, the activation function of the three gates is the sigmoid function to determine the information importance, which is denoted as $\boldsymbol{\sigma}$. The output of the gate ranges between 0 and 1. 0 denotes discard, while 1 indicates the information should be utilized.

To extract the relationship from the rolling ACE sequence by

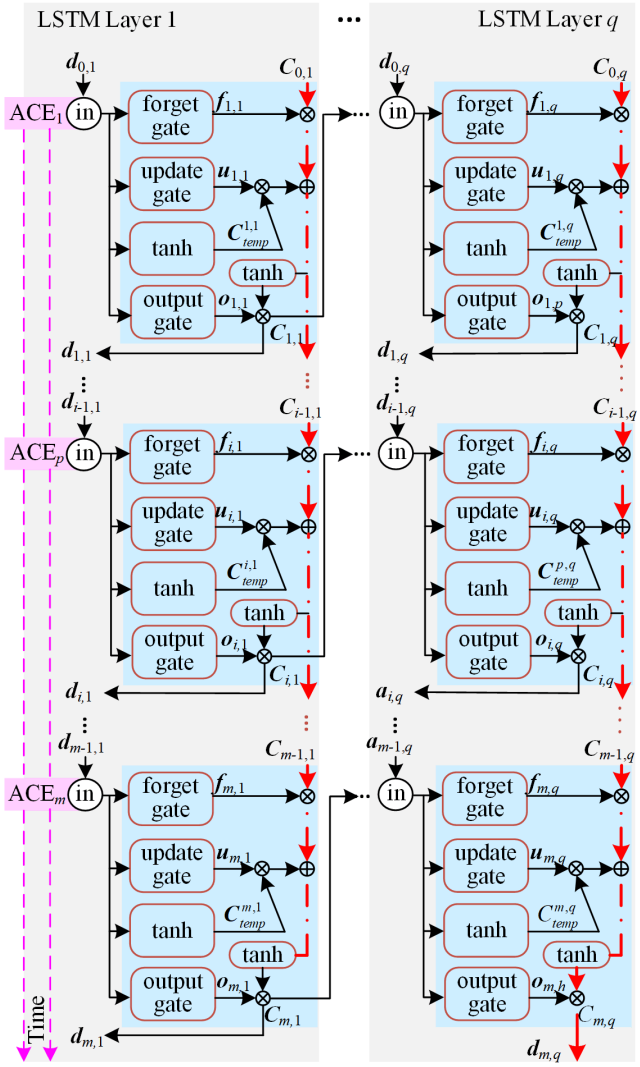


Fig. 4. Deep LSTM decoder array.

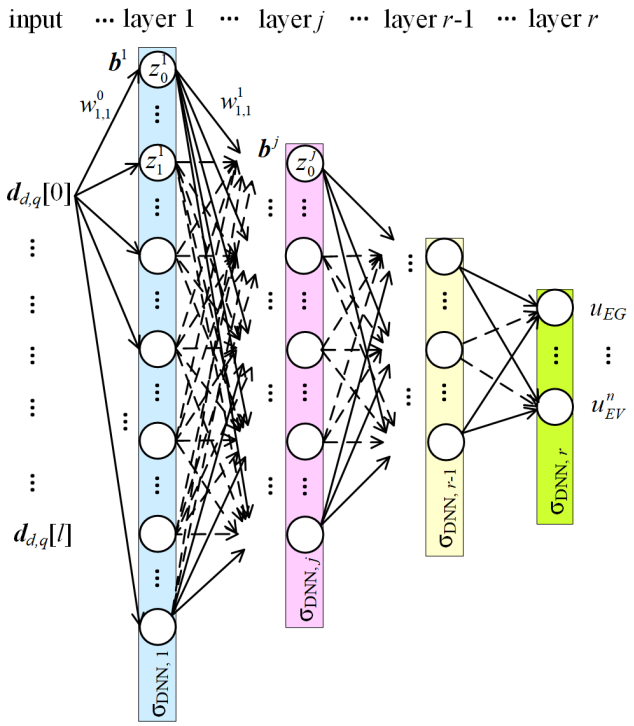


Fig. 5. Deep neural network dispatch array.

the neural network, the previous decoding information $\boldsymbol{d}_{p\text{-}1,q}$ is sequentially transmitted to the next decoding process at $t=p$ obtaining the next gate input $\boldsymbol{x}_{in}$ in (11). Without duplicate calculation, the inputs of three gates are the same

$$\boldsymbol{x}_{in} = \begin{bmatrix} \boldsymbol{d}_{p-1,q} & ACE_i \end{bmatrix}^T \tag{11}$$

Besides the real-time rolling, as another advantage of the LSTM network, the $ACE_i$ in (11) can be extended as a tensor input $\boldsymbol{ACE}_i$, which forms the rolling tensor input

$$\boldsymbol{ACE}_i = \begin{bmatrix} ACE_{i-T} & \cdots & \cdots & ACE_i \end{bmatrix} \tag{12}$$

Based on the rolling input $\boldsymbol{x}_{in}$, the forget gate of LSTM cell partially erases the unnecessary message in the cell formulating the transmitting memory $\boldsymbol{C}^f_{p,q}$. Meanwhile, the update gate extracts the useful cue $\boldsymbol{C}^u_{p,q}$ for the memory update. The historical memory $\boldsymbol{C}^f_{p,q}$ and the instant trait $\boldsymbol{C}^u_{p,q}$ are integrated forming the sequential decoding tensor $\boldsymbol{d}_{p,q}$

$$\boldsymbol{C}_{p,q} = \boldsymbol{C}^f_{p,q} + \boldsymbol{C}^u_{p,q} \tag{13}$$

$$\boldsymbol{d}_{p,q} = \boldsymbol{o}_{p,q} \times \tanh(\boldsymbol{C}_{p,q}) \tag{14}$$

where $\boldsymbol{o}_{p,q} = \boldsymbol{\sigma}(\boldsymbol{W}_o \boldsymbol{x}_{in} + \boldsymbol{b}_o)$ is the decoding coefficient. The formulation processes of transmitting memory $\boldsymbol{C}^f_{p,q}$ and transient update $\boldsymbol{C}^u_{p,q}$ are attached in Appendix B.

Through the conveyor belt indicated in the red line, the cell state $C_{p,q}$ runs straight down the entire chain with only some minor linear interactions, which guarantees long-term memory. In the meantime, the temporary fluctuation feature contributes to the cell state through gates consisted of the sigmoid neural net layer forming the decoding tensor in (14).

### *B. Intelligent Dispatch with DNN Array*

Absorbing the high-dimension decoding tensor from the deep LSTM-based decoder, the deep neural network is then deployed as a dispatch case in Fig. 5. The natural multiple inputs and multiple outputs feature makes a deep neural network suitable for the decision making of various subjects. Furthermore, the parallel computation capacity of GPU can be fully utilized with the combination of DNN, which improves the online performance.

From the $r$ layers DNN in Fig. 5, the input layer is made by the decoding tensor $\boldsymbol{d}_{p,q}$. Connecting with the DNN, the fluctuation information is broadcasted in the neural network. By a fully connected network, the $v^{th}$ node state in $j^{th}$ layer is

$$z^j_v = \sum_y w^{j-1}_{v,y} o^{j-1}_y + b^{j-1}_v \tag{15}$$

where $w^{j-1}_{v,y}$ is the weight between the $v^{th}$ node in $j^{th}$ layer and the $y^{th}$ node in $(j\text{-}1)^{th}$ layer, $b^{j-1}_v$ is the bias of $(j\text{-}1)^{th}$ layer.

Assuming the action function $\sigma_{DNN,j}$ in this corresponding layer, the output of this node is formulated as

$$o^{v,j}_{DNN} = \sigma_{DNN,j}(z^j_v) \tag{16}$$

Various action functions such as Leaky Rectified Linear Unit (Leaky ReLU) [32] could be used in (16). Summarizing (15)-(16), the dispatch command tensor for electrical grid or EV aggregators is successively produced

$$\boldsymbol{u}(t) = [u_{EG}, \boldsymbol{u}_{EV}]^T = \boldsymbol{\sigma}^{r-1}_{DNN}(\boldsymbol{z}^{r-1}) \tag{17}$$

### *C. Online Framework Evolution*

To avoid redundant offline training, a unified online evolution strategy is developed for the decoder-dispatch framework, which adjusts the network gradient based on the real-time operation. In this section, the optimization of instantaneous and relative frequency deviation is illustrated as an example. The rolling frequency fluctuation sequence propagates up to the hidden units at each layer and finally produces the power command for the EV aggregators and electrical grid. The next frequency status $\Delta f_t$ is then determined with the instantaneous variation

$$e_{in} = \|\Delta f_t\|_1 \tag{18}$$

where $\| \ \|_1$ is the L1 norm presented here as an example. To enhance the online stability, the loss of mean square error can

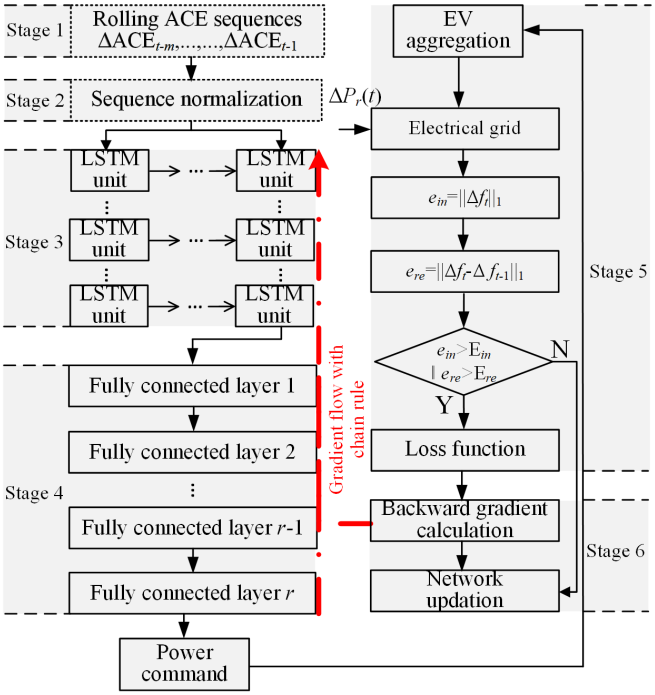


Fig. 6. Evolutionary decoder-dispatch framework.

also be adopted. Also, the relative dynamic is obtained

$$e_{re} = \left\| \Delta f_t - \Delta f_{t-1} \right\|_1 \tag{19}$$

Considering instantaneous and relative deviations [9], the loss function can be integrated combining these two parts

$$Loss = \omega_{in} e_{in} + \omega_{re} e_{re} \tag{20}$$

where $\omega_{in}$ and $\omega_{re}$ are the weights for the two kinds of errors.

The backpropagation algorithm firstly computes the gradient of the cost function. Based on the gradient calculated by the backpropagation algorithm, the optimization methods would then perform gradient-descent in an online manner. The derivation of framework gradient for the weights and biases are attached in Appendix C.

To achieve the online optimization gradient, various stochastic optimization approaches can be employed. Among them, Adam (adaptive moment estimation) is a method that only requires estimates of first and second moments of the gradients with little memory requirement [31]. Combining the advantages of adaptive gradient algorithm and root mean square propagation, the exponential moving averages of the gradient ($m_c$) and the squared gradient ($v_c$) are both deployed to adapt the parameter learning rates. The hyper-parameter $\beta_1 \in [0, 1)$ controls the exponential decay rates

$$m_c = \beta_1 m_{c-1} + (1-\beta_1) g_{c-1} \tag{21}$$

By $\beta_2 \in [0, 1)$, the second raw moment estimate is obtained as

$$v_c = \beta_2 v_{c-1} + (1-\beta_2) g_{c-1}^2 \tag{22}$$

TABLE I
ONLINE FRAMEWORK EVOLUTION ALGORITHM

| **Algorithm** | Online gradient evolution of decoder and dispatch |
|---|---|
| Input: | The dispatch command generated by the LSTM-DNN layers. |
| Output: | Network weight updation of LSTM array and DNN array. |
| 1 | Transfer the grid and EV regulation commands $u_{EG,t}$, $u_{EV,t}^k$ ($k$=1,2,…,$n$) to physical system; |
| 2 | Electrical grid and aggregated EVs generates the power $\Delta P_{EG,t}$, $\Delta P_{EV,t}^k$ ($k$=1,2,…,$n$) for the frequency regulation; |
| 3 | The electrical grid frequency responses according to power outputs and the renewable energy disturbance $\Delta P_{r,t}$; |
| 4 | The absolute frequency deviation is calculated $e_{in}=\|\Delta f_t\|$; |
| 5 | The relative frequency deviation is calculated $e_{re}=\|\Delta f_t - \Delta f_{t-1}\|$; |
| 6 | **If** $e_{in}$>Erro$_{in}$ \|\| $e_{re}$>Erro$_{re}$ (Erro$_{in}$ and Erro$_{re}$ are threshold values) |
| 7 | Construct the loss function $\omega_{in} e_{in} + \omega_{re} e_{re}$ based on the absolute and the relative deviations; |
| 9 | $c$:= $c$+1 |
| 10 | Get weight/bias gradients with $g_c \leftarrow \nabla_\theta Loss_c(\theta)$ |
| 11 | Update first moment estimate by $m_c \leftarrow \beta_1 m_{c-1} + (1-\beta_1) g_{c-1}$ |
| 12 | Update second moment estimate $v_c \leftarrow \beta_2 v_{c-1} + (1-\beta_2) g_{c-1}^2$ |
| 13 | Calculate the average-corrected with $\hat{m}_c \leftarrow m_c / (1-\beta_1^c)$ |
| 14 | Calculate the bias-corrected via $\hat{v}_c \leftarrow v_c / (1-\beta_2^c)$ |
| 15 | Parameter updation $\theta_c \leftarrow \theta_{c-1} - lr \cdot \hat{m}_c / (\sqrt{\hat{v}_c} + \varepsilon)$, ε is a very small number to prevent zero division, *lr* refers the learning rate |
| 16 | **End if** |

According to the average gradient and $\beta_1$, the moving average is corrected as

$$\hat{m}_c = m_c / (1-\beta_1^c) \tag{23}$$

Similarly, the bias-corrected second raw moment is derived

$$\hat{v}_c = v_c / (1-\beta_2^c) \tag{24}$$

With adjusted $\hat{m}_c$ and $\hat{v}_c$, network parameters are updated based on the real-time gradient. The pseudo-code of proposed algorithm for unified online adaption is given in Table I.

Summarizing Subsection A-C, the flowchart of the rolling decoder-dispatch framework is depicted in Fig. 6, which includes six implementation stages (rolling input, sequence normalization, LSTM decoding, DNN dispatch, loss generation, and online evolution).

### *D. Framework Design Workflow*

The parameters of LSTM and DNN are designed based on the following four procedures: framework structure establishment, LSTM array setting, DNN array setting, and value initialization.

➢ **Framework structure establishment:**

For a deep network framework, [33] pointed out that layers in the front of a network are used to extract the input feature, while the deep layers of the network tend to filter and combine the shallow features. Therefore, the node number of front layer is more than that of next layer, which makes the shape of whole neural network like a pyramid.

Following this principle, the whole LSTM-DNN structure is designed from the last layer. The node number of in the last

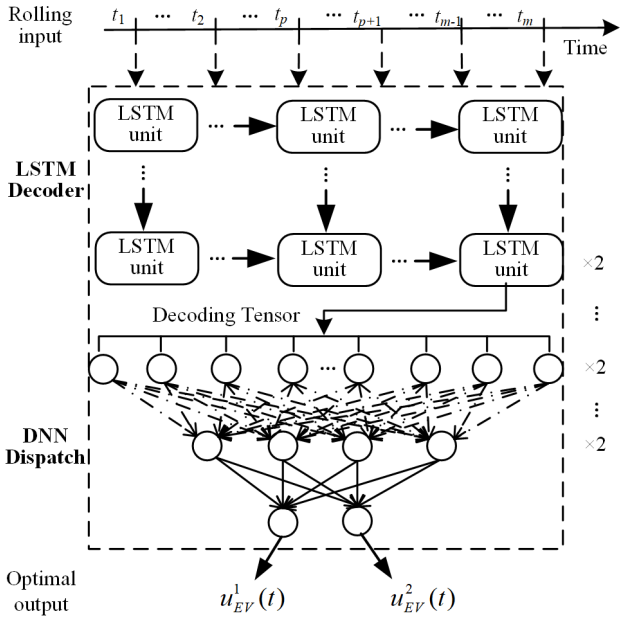


Fig. 7. Framework structure establishment.

layer of network is set the same with the number of EV aggregators. Multiplying by 2 successively, the node number of each layer is then calculated formulating a pyramid in Fig. 7.

➢ **DNN array setting:**

After the establishment of framework structure, the DNN array is further optimized for the online deployment. Considering the depth of neural network, the layer number of DNN should satisfy $L_{dnn}\geq 4$ for the enhancement of regulation performance. For the online efficiency, the DNN layer number could be either 5 with node number of (64, 32, 16, 8, 4) or 4 with node number of (32, 16, 8, 4). To compare these two options, the frequency waveform is presented in Fig. 8. From Fig. 8, the grid frequency performance does not improve when the layer number increases from 4 to 5. Hence, the DNN layer is set as $L_{dnn}=4$ to boost online efficiency.

➢ **LSTM array setting:**

The setting of LSTM array depends on the numbers of hidden layer nodes and layer. Because the secondary frequency regulation occurs in the timescale of 1-10 minutes [11], the node number $N_{lstm}$ of LSTM can be selected based on the timescale of minute. As the PV fluctuation data were measured every 1 second in [4], the minimum node number is $N_{min}$=1min/1second=60. To sufficiently utilize the capacity of

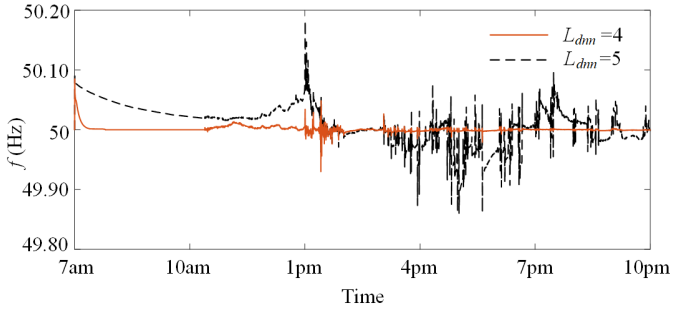


Fig. 8. DNN array setting test.

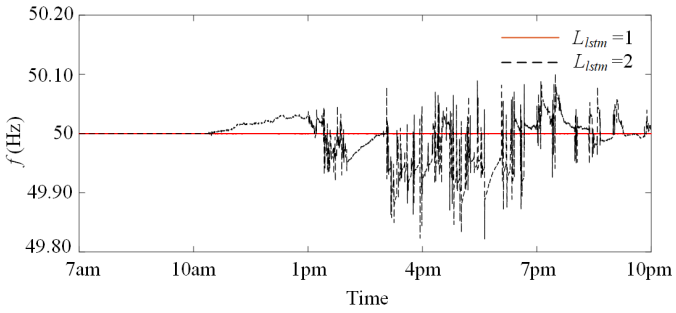


Fig. 9. LSTM array setting test.

LSTM, the hidden layer node is set at least twice of the minimum node number to extract the temporal feature from rolling 2 minutes, which means $N_{lstm}\geq 2N_{min}$. According to the existing research [34], the number of hidden layer is usually selected with $2^l$, $l$=1, 2, 3, …, for the convenient arrange of node number on other layers. Hence, the hidden layer node of LSTM is selected as $N_{lstm}=2^7=128\geq 120$. After the selection of hidden layer nodes, the layer number $L_{lstm}$ is tested from 1 to guarantee online efficiency. The frequency regulation results of layer number 1 and 2 are depicted in Fig. 9. As can be seen from Fig. 9, the frequency waveform at $L_{lstm}$ =1 is smoother than that of $L_{lstm}$ =2. It means that only one LSTM layer with the node number of 128 is adequate for the secondary frequency regulation. The gradient backpropagation may suffer from difficulties for this frequency regulation system when the LSTM decoder is very deep. The advantage of LSTM and DNN interconnection is also shown comparing Fig. 8 and 9.

➢ **Value initialization:**

After the selection of framework architecture, the initialization is another important factor affecting the regulation performance. Following the guidance of Pytorch [35], the uniform distribution is employed for the initialization task, which is expressed as

$$W,b\sim U(-bound,bound) \tag{25}$$

where $bound=\sqrt{1/f_{in}}$, $f_{in}$ is the input size of each network layer.

Following these four procedures, the framework structure, DNN array, and LSTM array, value initialization can be determined for the online frequency regulation.

## IV. Case Studies

### A. Validation System

In order to verify the effectiveness of the proposed decoder-dispatch framework for the hybrid vehicle-grid system, a power system model including two EV aggregators and the power plant dynamics is chosen. The typical values of the parameters are listed in Table II and the corresponding frequency performance is shown in Fig. 10. The grid frequency in Fig. 10 is maintained between 49.9Hz and 50.10Hz, which will not activate the action of regional transmission organization [36]. It should be noted that all parameters in

TABLE II
SYSTEM PARAMETERS

| Parameter | Symbol | Value |
|---|---|---|
| **Electric grid** | | |
| Turbine constant | $T_c$ | 0.3 |
| Reheat constant | $T_r$ | 12 |
| Turbine fraction | $F_p$ | 1/6 |
| Governor constant | $T_g$ | 0.2 |
| Inertia constant | $M$ | 8.8 |
| Damping coefficient | $D$ | 1 |
| Droop coefficient | $R$ | 1/4 |
| Bias factor | $\beta$ | 3 |
| Grid participation rate | $\alpha_0$ | 0.8 |
| Proportional gain | $K_P$ | 2 |
| Integral gain | $K_I$ | 1.6 |
| **Electric vehicle** | | |
| Aggregator 1 | $\alpha_1$ | 0.02 |
| Aggregator 2 | $\alpha_2$ | 0.18 |
| Charging/discharging coefficient | $K_{EA}^1$, $K_{EA}^2$ | 1 (kW / Hz) |
| Aggregation time constant | $T_{EA}^1$, $T_{EA}^2$ | 5 (s) |

Table II might vary during practical operation. Although Table II provides a fixed model and parameter values according to references, the real-time electrical-grid-electric-vehicle system is time-varying. The operating states of electrical grid and the aggregation states of electric vehicles are not the same all the time, which makes these parameter values uncertain during the practical operation. Therefore, without the dependence on the system model, this work develops the decoder-dispatch framework and online rolling evolution mechanism to actively learn the system variation and evolve during the operation. According to [37], the electrical grid in the frequency regulation system is represented by three parts: speed governor, turbine, rotating mass and load. The speed governor controls the admission of steam to the turbine. The stored energy of high-pressure and high-temperature steam is then converted into the rotating energy by a steam turbine, which combines with the power from renewable energies and electric vehicles. The rotating masses from grid generators provide the inertia $M$ to overcome the instant power imbalance. Because of motor loads in the power system, their electrical power changes with frequency due to the changes in motor speed, which introduces the damping coefficient $D$ in the power system. The PV measurement data on June 18-24, 2012 from Electric Power Research Institute are imported as the renewable energies [4]. 1-second resolution power data are implemented as the uncertainties to disturb the electrical grid frequency. As the damping coefficient $D$ also affects the steady-state frequency in the secondary frequency regulation, the damping dip of the

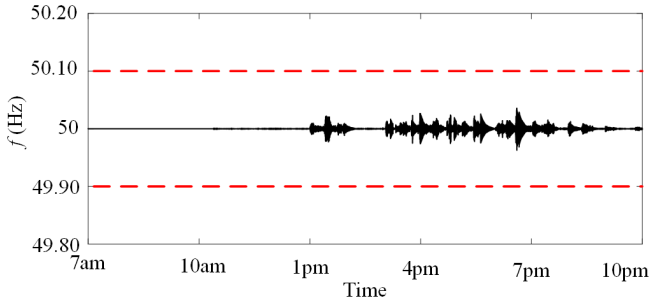


Fig. 10. The grid frequency without time-variations.

TABLE III
PARAMETERS OF LSTM-DNN ARRAY

| Parameter | Symbol | Value |
|---|---|---|
| Learning rate | $lr$ | 0.0002 |
| LSTM layer number | $L_{lstm}$ | 1 |
| LSTM hidden layer node | $N_{lstm}$ | 128 |
| DNN layer number | $L_{dnn}$ | 4 |
| DNN hidden layer node | $N_{dnn}$ | (32, 16, 8, 4) |
| Leaky ReLU slope | $\alpha$ | 0.01 |
| Absolute error threshold | $Erro_{in}$ | 1e-6 |
| Relative error threshold | $Erro_{in}$ | 1e-4 |
| Denominator threshold | $\varepsilon$ | 1e-8 |
| Decay rate of first moment | $\beta_1$ | 0.9 |
| Decay rate of second moment | $\beta_2$ | 0.99 |

power system is tested as another uncertainty for the proposed method. The parameters of the electric vehicles are selected from [30]. Considering the time delay during the EV aggregation, the EV aggregation time is varied from 0.1s to 10s to validate the dispatch framework.

The whole decoder-dispatch network and algorithm, as shown in Fig. 3 and Fig. 6-7, are programmed and implemented with Pytorch on a desktop computer with a 3.8 GHz Intel i7600 processor and 16GB of memory. To implement the developed scheme, the system is further deployed on NVIDIA 2080Ti GPU and CUDA deep neural network library for the real-time dispatch.

### *B. Time-varying Electrical Grid*

During the real-time operation, all the electrical grid parameters might suffer from different variations, which challenges the uniform parameter setting in traditional dispatch methods. Without offline tuning, according to the proposed framework in Section II-III, a decoder-dispatch network is established with one-layer LSTM array and four-layer DNN as an example. The hidden nodes in LSTM is 128, while there are 32, 16, 8, 4 nodes in the four DNN layers. The Leaky ReLU is selected as the activation function of DNN with a small slope $\alpha$=0.01. The rolling inputs for the decoder are extended to 10 sequences for the better versatility, and the learning rate during the online evolution is 0.0002. $\omega_{in}$ and $\omega_{re}$ are set the same value 1. $\omega_{in}$ can also be adjusted to 10 for the fast evolution facing small frequency deviations. The parameters of LSTM-DNN array are summarized in Table III. Facing the solar disturbance of 17 June, the frequency fluctuations of a conventional electrical-grid-electric-vehicle system with traditional PI controller and the proposed decoder-dispatch framework are depicted in Fig. 11.

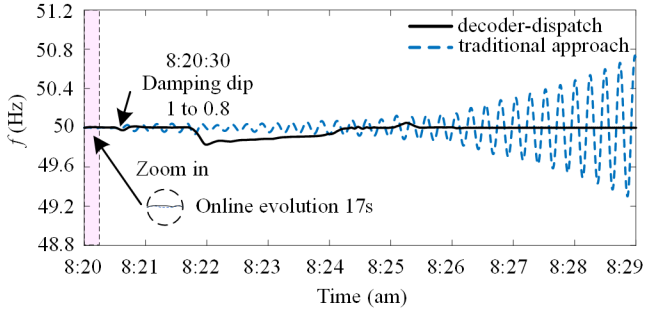


Fig. 11. The frequency variations with the real-time damping variation.

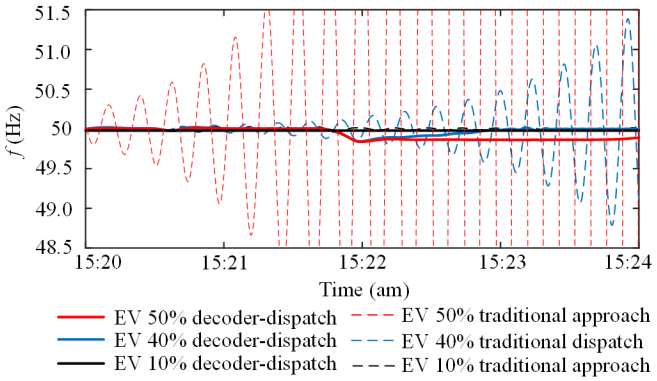


Fig. 12. Frequency waveforms of changing EV participation ratios.

As shown in Fig. 11, without any offline training, the proposed framework requires only 17s to learn the system online, which reaches the same performance as the traditional dispatch method after the pink area. At 15:20:30, a slight dip of system damping $D$ from 1 to 0.8 is assumed to present the real-time electrical grid dynamic. Because of this small internal disturbance, the $f$ oscillation increases to 50.74Hz at 15:29 am under the traditional error elimination approach. However, the new dispatch method maintains the frequency stability with the maximum deviation of only 0.17Hz.

As the time-varying penetration level of electric vehicles, the participation ratio $a_0$ is defined as the output power ratio between electric vehicles and the electrical grid [30], which indicates the EV penetration level. Setting this time-varying coefficient to 10%, 40%, and 50%, the frequency regulation results are depicted in Fig. 12. It can be seen that the coordination between electrical grid and electric vehicles are boosted through the proposed method. The EV participation rate is able to reach 50% due to the online framework, while the system frequency would violate ±1 Hz under the previous approach.

### C. *Time-varying Electric Vehicle Aggregation*

Apart from the variation in the electrical grid, the aggregation status of electric vehicles is also affecting the whole system. To investigate the impact of aggregation time, the time coefficient $T_{EA}$ is changed from 0.1 to 10 in Fig. 13. The smooth waveforms indicate that the decoder-dispatch system can adjust well to the electric-vehicle dynamics, which restores the frequency between 48.8Hz and 50.2Hz.

Furthermore, the PV fluctuation and corresponding power commands generated by proposed and traditional methods are presented in Fig. 14 to further explore the advantage of

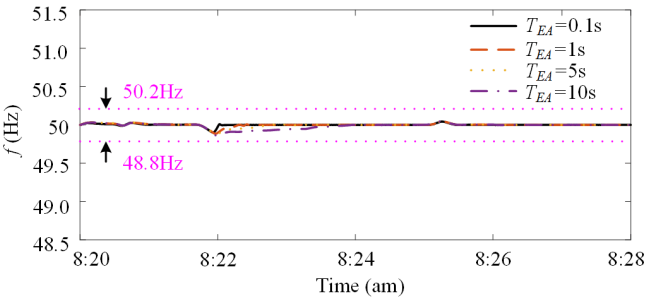


Fig. 13. The frequency variations with various vehicle aggregation time.

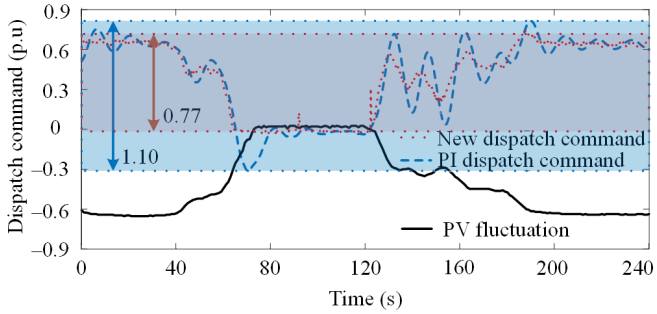


Fig. 14. The dispatch command comparisons facing the PV fluctuation.

proposed strategy under $T_{EA}^1 = T_{EA}^2 = 0.1$s . Suffering a 0.68p.u. PV disturbance, the proposed dispatch method decodes the variation trend and compresses the power command with 0.77p.u. By contrast, the traditional dispatch signal varies according to the external disturbance without the decoding mechanism, which requires an extra 0.33p.u. power.

### D. *Evolution and Compatibility with the Existing Approach*

Because of the rolling inputs and online evolution algorithm, the dispatch center based on the LSTM-DNN is constantly learning, as shown in Fig. 15. After learning the first operation, the re-loaded system model can rapidly get used to the environment. Facing the disturbance between 15:36 am to 15:38 am, without any learning, the proposed method prevents the system frequency from falling below point A (49.83 Hz). Once this scenario is learned, the framework is able to stop the frequency from falling below Point B (49.91Hz) under the same scenario. By learning only four times, the deviation is reduced to 0.005 Hz.

To detect the compatibility of the proposed method with the existing method, the decoder-dispatch system is deployed as the EV dispatch center, while the PI controller manages the conventional regulation system. It can be seen from Fig. 16 that the online decoder-dispatch network works well with the conventional one. Compared with Fig. 10, the mean square error is decreased from 0.00675 to 0.00000292. To further illustrate the regulation improvement, the single-hidden-layer neural network of fixed parameters trained offline in [21] is employed for the comparison. According to its regulated waveform in Fig. 17, the grid frequency is controlled within 49.90Hz and 50.10Hz by the hierarchical adaptive control strategy. The mean square error of frequency fluctuation in Fig. 17 is 0.0017, which is still much larger than that of the proposed framework.

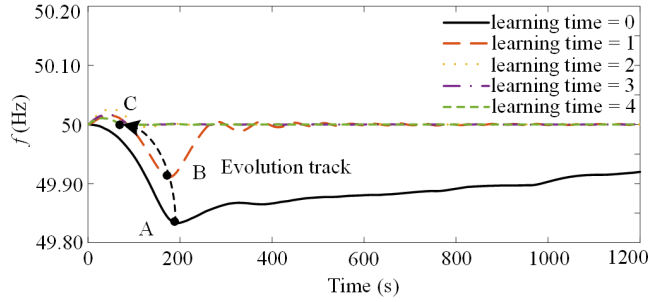


Fig. 15. The evolution track of decoder-dispatch framework.

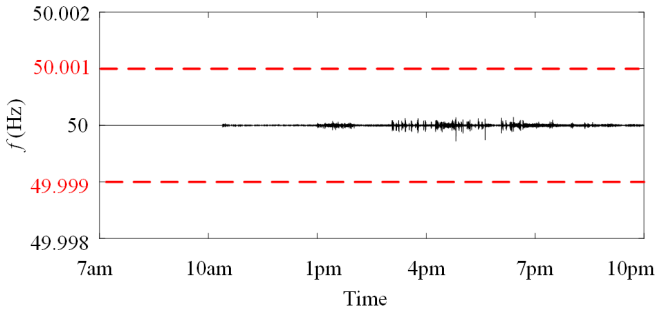


Fig. 16. The dispatch compatibility with the existing approach.

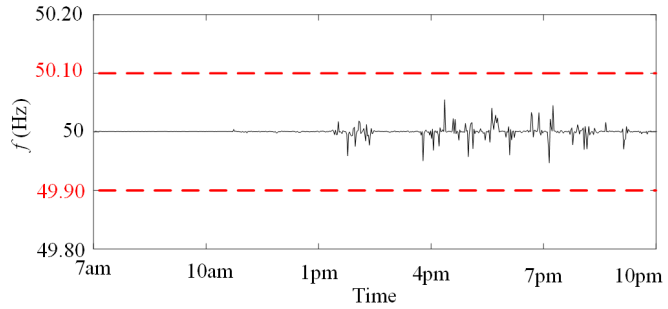


Fig. 17. The frequency regulated by the method in [21].

### E. *GPU and CPU Deployments*

Deploying the developed framework on a 2080Ti GPU, the sequential command generation for the 24h of 17 June takes only 55min02s. For each dispatch command, the average computation time is 3.78ms. The dispatching efficiency when applying to PV measurement data on other days is shown in Table III. The corresponding calculation time by Intel(R) Core(TM) i7-7500U CPU is also attached.

Regardless of external disturbances, the computation time remains stable as seen in Table III for both GPU and CPU. The GPU averagely takes 3.79ms to generate each dispatch command, while the average calculation time with Intel(R) Core(TM) i7-7500U CPU is 10.55ms.

### F. *Robustness Test*

Besides the existing validation on June 17, the selected parameters of the LSTM-DNN framework are further tested on the PV datasets of June 18-June 24. The dispatch performance and comparison with DNN are shown in Fig. 18-24.

From Fig. 18-24, it can be seen that the designed parameters are robust facing the various fluctuations from renewable energy. On these seven-day datasets, the proposed decoder-dispatch framework achieves the competent waveforms regardless of the external uncertainties. To quantitatively investigate the improvement brought by the developed framework, the mean square errors and the

TABLE III AVERAGE CALCULATION TIME OF EACH DISPATCH COMMAND ON DIFFERENT DAYS

| June | 18 | 19 | 20 | 21 | 22 | 23 | 24 |
|---|---|---|---|---|---|---|---|
| CPU (ms) | 10.52 | 10.87 | 10.30 | 10.33 | 10.55 | 10.70 | 10.55 |
| GPU (ms) | 3.78 | 3.80 | 3.83 | 3.77 | 3.75 | 3.79 | 3.84 |

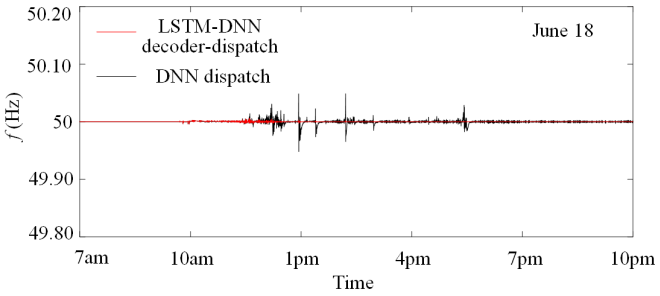


Fig. 18. The dispatch performance on June 18 dataset..

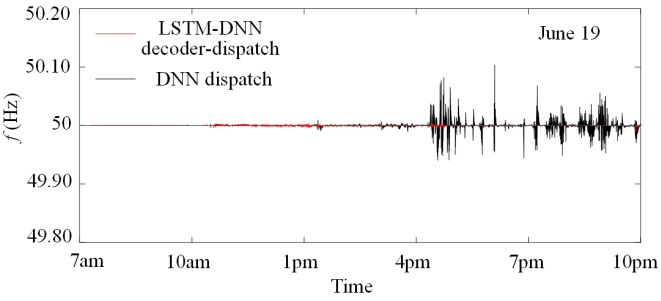


Fig. 19. The dispatch performance on June 19 dataset..

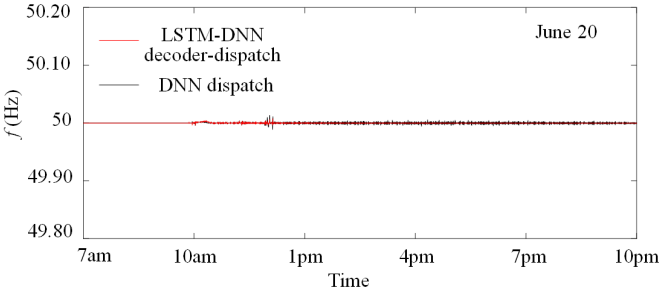


Fig. 20. The dispatch performance on June 20 dataset..

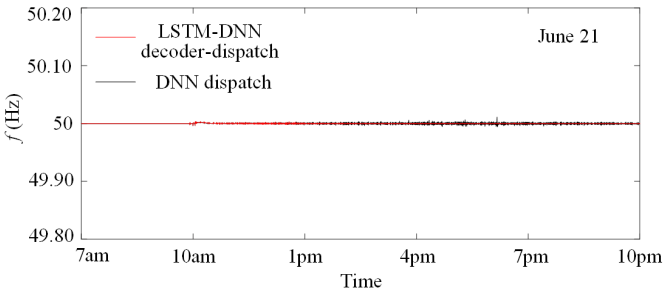


Fig. 21. The dispatch performance on June 21 dataset..

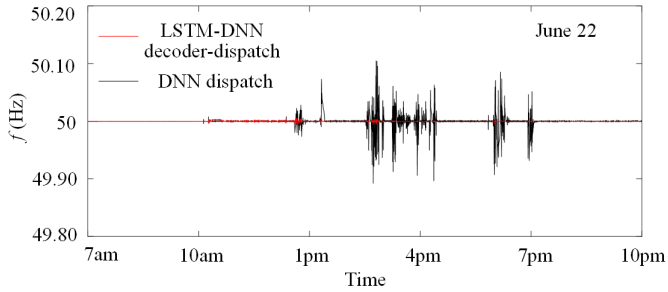


Fig. 22. The dispatch performance on June 22 dataset..

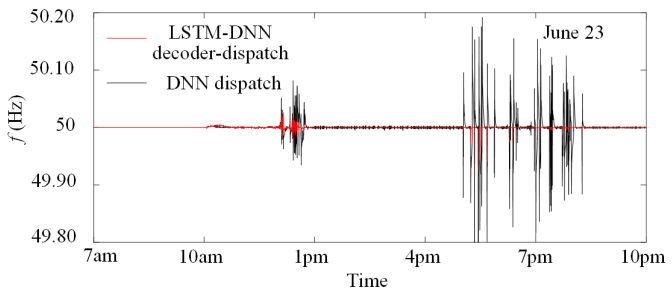


Fig. 23. The dispatch performance on June 23 dataset..

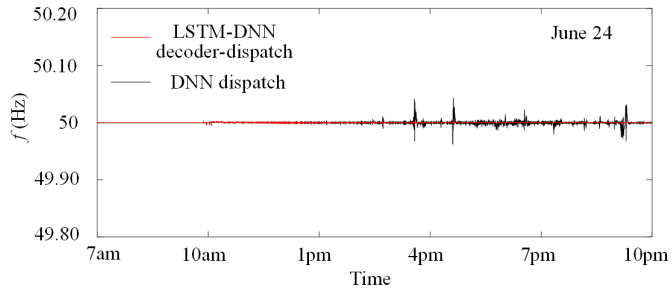


Fig. 24. The dispatch performance on June 24 dataset..

maximum frequency deviations are listed in Table IV and Table V, respectively. According to Table IV, the mean square error varies between 1.49e-7 and 3.28e-7 for the decoder-dispatch framework of LSTM-DNN array, while the variation range is [8.83e-7, 2.59e-4] for DNN dispatch. The maximum error of DNN dispatch is 2.59e-4 on June 23, which is 790 times the error of LSTM-DNN on the same day. From Table V, it can be seen that the maximum frequency deviation regulated by the LSTM-DNN framework is only 0.0843Hz, but the maximum deviation is 0.2194Hz with only DNN dispatch. Not only can the robustness of the proposed framework be seen from these tests, but the effectiveness of LSTM decoder is also demonstrated.

TABLE IV
MEAN SQUARE ERRORS ON DIFFERENT DATASETS

| June | DNN dispatch | Decoder-dispatch framework with LSTM-DNN array (Hz) |
|---|---|---|
| **June 18** | 7.41e-6 | 1.77e-7 |
| **June 19** | 7.86e-6 | 1.83e-7 |
| **June 20** | 9.98e-7 | 2.29e-7 |
| **June 21** | 8.83e-7 | 1.46e-7 |
| **June 22** | 7.26e-6 | 2.47e-7 |
| **June 23** | 2.59e-4 | 3.28e-7 |
| **June 24** | 7.97e-6 | 1.49e-7 |

TABLE V
MAXIMUM FREQUENCY DEVIATIONS ON DIFFERENT DATASETS

| June | DNN dispatch (Hz) | Decoder-dispatch framework with LSTM-DNN array (Hz) |
|---|---|---|
| **June 18** | 0.0520 | 0.0057 |
| **June 19** | 0.1037 | 0.0097 |
| **June 20** | 0.0135 | 0.0078 |
| **June 21** | 0.0113 | 0.0037 |
| **June 22** | 0.1078 | 0.0062 |
| **June 23** | 0.2194 | 0.0843 |
| **June 24** | 0.0427 | 0.0046 |

## V. CONCLUSIONS

To address the time-varying and stochastic nature of renewable energy and electric-vehicle aggregation, an online rolling decoder-dispatch framework has been proposed for the frequency management of electrical-grid-electric-vehicle systems. Through decoding the time-sequential cues with long-short-term memory (LSTM) array, the turbulence discipline is mapped into a high-dimension tensor, which feeds the multiple input interface of deep neural network (DNN) array. Offline training is avoided by online gradient adjustment implemented on the graphics processing unit (GPU).

Numerical studies demonstrate improved regulation performance when the decoder-dispatch method faces internal and external system variations. The continuous evolution and the compatibility with the existing system are also presented, as well as the implementation performance on GPU and CPU. According to the demonstration example of deep learning, the further investigation in decoder array, dispatch array, decoder-dispatch interface, evolutionary algorithm, and online memory update could be implemented to establish a real intelligent frequency management system.

## APPENDIX A

The time-varying coefficients in (10) are

$$\boldsymbol{A}=\begin{bmatrix} \frac{-D(t)}{M(t)} & \frac{1}{M(t)} & 0 & 0 & 0 & \frac{1}{M(t)} & \cdots & \frac{1}{M(t)} \\ 0 & \frac{-1}{T_c(t)} & \frac{1}{T_c(t)} & 0 & 0 & 0 & \cdots & 0 \\ \frac{-F_p(t)}{R(t)T_g(t)} & 0 & \frac{-1}{T_c(t)} & \frac{T_g(t)-F_p(t)T_r(t)}{T_r(t)T_g(t)} & 0 & 0 & \cdots & 0 \\ \frac{-1}{R(t)T_g(t)} & 0 & 0 & \frac{-1}{T_g(t)} & 0 & 0 & \cdots & 0 \\ \beta & 0 & 0 & 0 & 0 & 0 & \cdots & 0 \\ 0 & 0 & 0 & 0 & 0 & \frac{-1}{T_{EV}^1(t)} & \cdots & 0 \\ \vdots & \vdots & \vdots & \vdots & \vdots & \vdots & \ddots & \vdots \\ 0 & 0 & 0 & 0 & 0 & 0 & \cdots & \frac{-1}{T_{EV}^n(t)} \end{bmatrix} \quad \text{(A1)}$$

$$\boldsymbol{B}=\begin{bmatrix} 0 & 0 & \frac{F_p(t)\alpha_0}{T_g(t)} & \frac{\alpha_0}{T_g(t)} & 0 & \cdots & 0 \\ 0 & 0 & 0 & 0 & \frac{\alpha_1 K_{EV}^1(t)}{T_{EV}^1(t)} & \cdots & \frac{\alpha_n K_{EV}^n(t)}{T_{EV}^n(t)} \end{bmatrix}^T \quad \text{(A2)}$$

$$\boldsymbol{F}=[1/M(t),0,0,0,0,...,0,...0]^T \quad \text{(A3)}$$

## APPENDIX B

The forget gate partially erases the unnecessary message in the cell via Hadamard product

$$\boldsymbol{f}_{p,q}=\boldsymbol{\sigma}(\boldsymbol{W}_f^{p,q}\boldsymbol{x}_{in}+\boldsymbol{b}_f) \quad \text{(B1)}$$

$$\boldsymbol{C}_{p,q}^f=\boldsymbol{f}_{p,q}\times\boldsymbol{C}_{p-1,q} \quad \text{(B2)}$$

where $\boldsymbol{f}_{p,q}$ is the forget gate output of $q^{\text{th}}$ LSTM layer at $t=p$, $\boldsymbol{C}_{p,q}^{f}$ is the transmitting memory.

The update gate selects the useful cue $\boldsymbol{C}_{p,q}^{u}$ for the update of cell memory

$$\boldsymbol{C}_{temp}^{p,q} = \tanh(\boldsymbol{W}_c \boldsymbol{x}_{in} + \boldsymbol{b}_c) \tag{B3}$$

$$\boldsymbol{u}_{p,q} = \boldsymbol{\sigma}(\boldsymbol{W}_u \boldsymbol{x}_{in} + \boldsymbol{b}_u) \tag{B4}$$

$$\boldsymbol{C}_{p,q}^{u} = \boldsymbol{u}_{p,q} \times \boldsymbol{C}_{temp}^{p,q} \tag{B5}$$

where $\boldsymbol{C}_{temp}^{p,q}$ presents all the new input details and $\tanh(x) = (e^{x} - e^{-x}) / (e^{x} + e^{-x})$ is the activation function.

## APPENDIX C

The loss contribution of $p^{th}$ node in the $j^{th}$ layer is

$$\delta_p^j = \partial Loss / \partial z_p^j \tag{C1}$$

Substituting the dispatch command to (C1), the node donation of the last layer is determined with the chain rule

$$\delta_p^r = (\partial Loss / \partial o_p^r) \cdot (\partial o_p^r / \partial z_p^r) \tag{C2}$$

For the node not in the last layer, its loss relation between the $p^{th}$ node in $j^{th}$ layer and the $q^{th}$ node in $(j+1)^{th}$ layer is

$$\begin{aligned} \delta_p^j &= \frac{\partial Loss}{\partial z_p^j} = \sum_q \frac{\partial Loss}{\partial z_q^{j+1}} \cdot \frac{\partial z_q^{j+1}}{\partial o_p^j} \cdot \frac{\partial o_p^j}{\partial z_p^j} \\ &= \sum_q \delta_q^{j+1} \cdot w_{q,p}^{j+1} \cdot \sigma_{DNN,j}((z_p^j) \end{aligned} \tag{C3}$$

With (C2)-(C3), the relationship between each node and the system loss is established. The weight gradient is formed as

$$\nabla_{w_{p,q}^j} Loss = \frac{\partial Loss}{\partial z_p^j} \cdot \frac{\partial z_p^j}{\partial w_{p,q}^j} = \delta_p^j \sigma_{DNN,j-1} \tag{C4}$$

Similarly, the gradient of bias $b_p^j$ is

$$\nabla_{b_p^j} Loss = \frac{\partial Loss}{\partial z_p^j} \cdot \frac{\partial z_p^j}{\partial b_p^j} = \delta_p^j \tag{C5}$$

According to the backpropagation algorithm above, the current gradient of the loss function is obtained with $\theta$ as the set of network parameters

$$g_c = \nabla_\theta Loss(\theta) \tag{C6}$$

## REFERENCES


[1] B., Kroposki, B. Johnson, Y. Zhang, V. Gevorgian, P. Denholm, B. M. Hodge, and B. Hannegan. "Achieving a 100% renewable grid: operating electric power systems with extremely high levels of variable renewable energy," *IEEE Power Energy Mag.*, vol. 15, no. 2, pp. 61-73, March 2017.

[2] Germany: federal ministry for economic affairs and energy, "The energy of the future: sixth energy transition monitoring report — summary," 2016. [Online]. Available: https://www.bmwi.de/Redaktion/EN/Publikationen/Energie/sechster-monitoring-bericht-zur-energiewende-kurzfassung.html.

[3] Danish Energy Agency, "Denmark's energy and climate outlook," 2018. [Online]. Available: https://ens.dk/en/our-services/projections-and-models/denmarks-energy-and-climate-outlook.

[4] Electric Power Research Institute, "Distributed PV monitoring and feeder analysis," 2012. [Online]. Available: https://dpv.epri.com/#targetText=EPRI%20then%20processes%20and%20manages,on%20utility%20operations%20and%20planning.&targetText=Here%2C%20you%20can%20learn%20about,variety%20of%20distributed%20PV%20systems.

[5] K. Hou, X. Xu, H. Jia, X. Yu, T. Jiang, K. Zhang, and B. Shu, "A reliability assessment approach for integrated transportation and electrical power systems incorporating electric vehicles," *IEEE Trans. Smart Grid*, vol. 9, no. 1, pp. 88-100, Jan. 2018.

[6] State Council of Republic of China State, "The national medium-and long-term program for science and technology development (2006-2020)," [Online]. Available: https://www.itu.int/en/ITU-D/Cybersecurity/Documents/National_Strategies_Repository/China_2006.pdf.

[7] Y. Mu, J. Wu, N. Jenkins, H. Jia, and C. Wang, "A spatial-temporal model for grid impact analysis of plug-in electric vehicles," *Applied Energy*, vol. 114, pp: 456-465, Feb. 2014.

[8] A. H. Ranjbar, A. Banaei, A. Khoobroo, and B. Fahimi, "Online estimation of state of charge in Li-ion batteries using impulse response concept," *IEEE Trans. Smart Grid*, vol. 3, no. 1, pp.360-367, March 2012.

[9] R. Wang, Q. Sun, D. Ma and Z. Liu, "The small-signal stability analysis of the droop-controlled converter in electromagnetic timescale," *IEEE Trans. Sustain. Energy*, vol. 10, no. 3, pp. 1459-1469, July 2019.

[10] The Guardian, "National Grid had three blackout near misses in three months," 2019. [Online]. Available: https://www.theguardian.com/business/2019/aug/12/three-blackout-near-misses-in-three-months-says-national-grid#targetText=Industry%20sources%20have%20confirmed%20that,frequency%20slumped%20to%2048.88Hz.

[11] Primary Frequency Response Senior Task Force, "Primary frequency response stakeholder education part 1 of 2," 2017. [Online]. Available: https://www.pjm.com/~/media/committees-groups/task-forces/pfrstf/20170901/20170901-primary-frequency-response-education-part-1-of-2.ashx.

[12] C. Dong, Q. Xiao, M. Wang, T. Morstyn, M. McCulloch and H. Jia, "Distorted stability space and instability triggering mechanism of EV aggregation delays in the secondary frequency regulation of electrical grid electric vehicle system," *IEEE Trans. Smart Grid*, in press.

[13] H. Jia, X. Li, Y. Mu, C. Xu, Y. Jiang, X. Yu, J. Wu, and C. Dong, "Coordinated control for EV aggregators and power plants in frequency regulation considering time-varying delays," *Applied Energy*, vol. 210, pp. 1363-1376, Jan. 2018.

[14] C. Peng, J. Zou, L. Lian, and L. Li, "An optimal dispatching strategy for V2G aggregator participating in supplementary frequency regulation considering EV driving demand and aggregator's benefits," *Applied Energy*, vol. 190, pp: 591-599, March 2017.

[15] S. Saxena, and Y. V. Hote, "Load frequency control in power systems via internal model control scheme and model-order reduction," *IEEE Trans. Power Syst.*, vol. 28, no. 3, pp. 2749-2757, Aug. 2013.

[16] S. Sönmez, and S. Ayasun, "Stability region in the parameter space of PI controller for a single-area load frequency control system with time delay," *IEEE Trans. Power Syst.*, vol. 31, no. 1, pp. 829-830, Jan. 2016.

[17] C. Mu, Y. Tang, and H. He, "Improved sliding mode design for load frequency control of power system integrated an adaptive learning strategy," *IEEE Trans. Ind. Electron.*, vol. 64, no. 8, pp. 6742-6751, Aug. 2017.

[18] H. A. Yousef, K. AL-Kharusi, M. H. Albadi, and N. Hosseinzadeh, "Load frequency control of a multi-area power system: An adaptive fuzzy logic approach," *IEEE Trans. Power Syst.*, vol. 29, no. 4, pp. 1822-1830, July 2014.

[19] S. F. Aliabadi, S. A. Taher, and M. Shahidehpour, "Smart deregulated grid frequency control in presence of renewable energy resources by EVs charging control," *IEEE Trans. Smart Grid*, vol. 9, no. 2, pp. 1073-1085, March 2018.

[20] S. Falahati, S. A. Taher and M. Shahidehpour, "Grid secondary frequency control by optimized fuzzy control of electric vehicles," *IEEE Trans. Smart Grid*, vol. 9, no. 6, pp. 5613-5621, Nov. 2018.

[21] C. Mu, W. Liu and W. Xu, "Hierarchically adaptive frequency control for an EV-integrated smart grid with renewable energy," *IEEE Trans. Ind. Inform.*, vol. 14, no. 9, pp. 4254-4263, Sept. 2018.

[22] S. Hochreiter, and J. Schmidhuber, "Long short-term memory." *Neural Comput.*, vol. 9, no. 8: pp. 1735-1780, Nov. 1997.
[23] S. Wen, Y. Wang, Y. Tang, Y. Xu, P. Li, and T. Zhao, "Real-time identification of power fluctuations based on LSTM recurrent neural network: a case study on Singapore power system," *IEEE Trans. Ind. Informat.*, vol. 15, no. 9, pp. 4254-4263, Sept. 2019.
[24] W. Kong, Z. Dong, Y. Jia, D. Hill, Y. Xu, and Y. Zhang, "Short-term residential load forecasting based on LSTM recurrent neural network," *IEEE Trans. Smart Grid*, vol. 10, no. 1, pp. 841-851, Jan. 2019.
[25] P. Zeng, H. Li, H. He, and S. Li, "Dynamic energy management of a microgrid using approximate dynamic programming and deep recurrent neural network learning," *IEEE Trans. Smart Grid*, vol. 10, no. 4, pp. 4435-4445, July 2019.
[26] Y. Du, and F. Li, "Intelligent multi-microgrid energy management based on deep neural network and model-free reinforcement learning," *IEEE Trans. Smart Grid*, vol. 11, no. 2, pp. 1066-1076, March 2020.
[27] C. Ren, and Y. Xu, "A fully data-driven method based on generative adversarial networks for power system dynamic security assessment with missing data," *IEEE Trans. Power Syst.*, vol. 34, no. 6, pp. 5044-5052, Nov. 2019.
[28] X. Li, F. Li, H. Yuan, H. Cui, and Q. Hu, "GPU-based fast decoupled power flow with preconditioned iterative solver and inexact newton method," *IEEE Trans. Power Syst.*, vol. 32, no. 4, pp. 2695-2703, July 2017.
[29] X. Li, and F. Li, "GPU-based power flow analysis with Chebyshev preconditioner and conjugate gradient method," *Electr. Power Syst. Res*, vol. 116, pp. 87-93, Nov. 2014
[30] K. S. Ko, and D. K. Sung, "The effect of EV aggregators with time-varying delays on the stability of a load frequency control system," *IEEE Trans. Power Syst.*, vol. 33, no. 1, pp. 669-680, Jan. 2018.
[31] D. Kingma, and J. Ba, "Adam: a method for stochastic optimization," in *Proc. ICLR*, San Diego, CA, USA, 2015, pp. 1-15.
[32] A. Maas, A. Hannun, and A. Ng. Rectifier nonlinearities improve neural network acoustic models. *Proc. ICML*, vol. 30, no. 1, pp. 1-6, 2013.
[33] M. D. Zeiler and R. Fergus, "Visualizing and understanding convolutional networks," in *Proc. ECCV*, Zurich, Switzerland, 2014, pp. 818-833.
[34] Y. Shi, K. Yao, L. Tian, and D. Jiang, "Deep LSTM based feature mapping for query classification," in *Proc. ECCV NAACL HLT*, San Diego, CA, USA, 2016, pp. 1501-1511.
[35] Pytorch, "Torch.nn.init," 2019. [Online]. Available: https://pytorch.org/docs/stable/_modules/torch/nn/init.html#calculate_gain.
[36] R. Wang, Q. Sun, X. Liu and D. Ma, "Power flow calculation based on local controller impedance features for the AC microgrid with distributed generations," *IET Energy Systems Integration*, vol. 1, no. 3, pp. 202-209, Sep, 2019.
[37] P. Kundur. *Power system stability and control*. New York, NY, USA: McGraw-Hill, 1994, pp. 589–599.

**Chaoyu Dong** received the B.Sc. degree in electrical engineering from Tianjin University, China, in 2013. He is also an academic visitor with the Department of Engineering Science at the University of Oxford.

His research interests include energy-information system stability and intelligent management.

**Ronghe Chu** received the B.S. in electrical engineering from Tianjin University of Science & Technology, Tianjin, China, in 2019. He is currently working towards the M.S. degree at Tianjin University, Tianjin, China.

His research interests include machine learning, computer vision, and applied research.

**Thomas Morstyn** (S'14-M'16) received the BEng (Hon.) degree from the University of Melbourne in 2011, and the PhD degree from the University of New South Wales in 2016, both in electrical engineering.

He is a Lecturer in Power Electronics and Smart Grids with the School of Engineering at the University of Edinburgh. He is also a visiting fellow with the Oxford Martin School at the University of Oxford. His research interests include multi-agent control and market design for integrating distributed energy resources into power system operations.

**Malcolm D. McCulloch** (SM'89) received the B.Sc. (Eng.) and Ph.D. degrees in electrical engineering from the University of the Witwatersrand, Johannesburg, South Africa, in 1986 and 1990, respectively.

In 1993, he joined the University of Oxford, Oxford, U.K., to head up the Energy and Power Group, where he is currently an Associate Professor in the Department of Engineering Science. He is active in the areas of electrical machines, transport, and smart grids. His work addresses transforming existing power networks, designing new power networks for the developing world, developing new technology for electric vehicles, and developing approaches to integrated mobility.

**Hongjie Jia** (M'04-SM'17) received the B.S., M.S., and Ph.D. degrees in electrical engineering from Tianjin University, Tianjin, China, in 1996, 1999, and 2001, respectively.

He is currently a Professor with Tianjin University, Tianjin, China. His research interests include power reliability assessment, stability analysis and control, distribution network planning and automation, and integrated energy system.